Self-Assembly

DOI: 10.1002/anie.201007388

Mapping the Sequential Self-Assembly of Heterometallic Clusters: From a Helix to a Grid**

Graham N. Newton, Tatsuya Onuki, Takuya Shiga, Mao Noguchi, Takuto Matsumoto, Jennifer S. Mathieson, Masayuki Nihei, Motohiro Nakano, Leroy Cronin, and Hiroki Oshio**

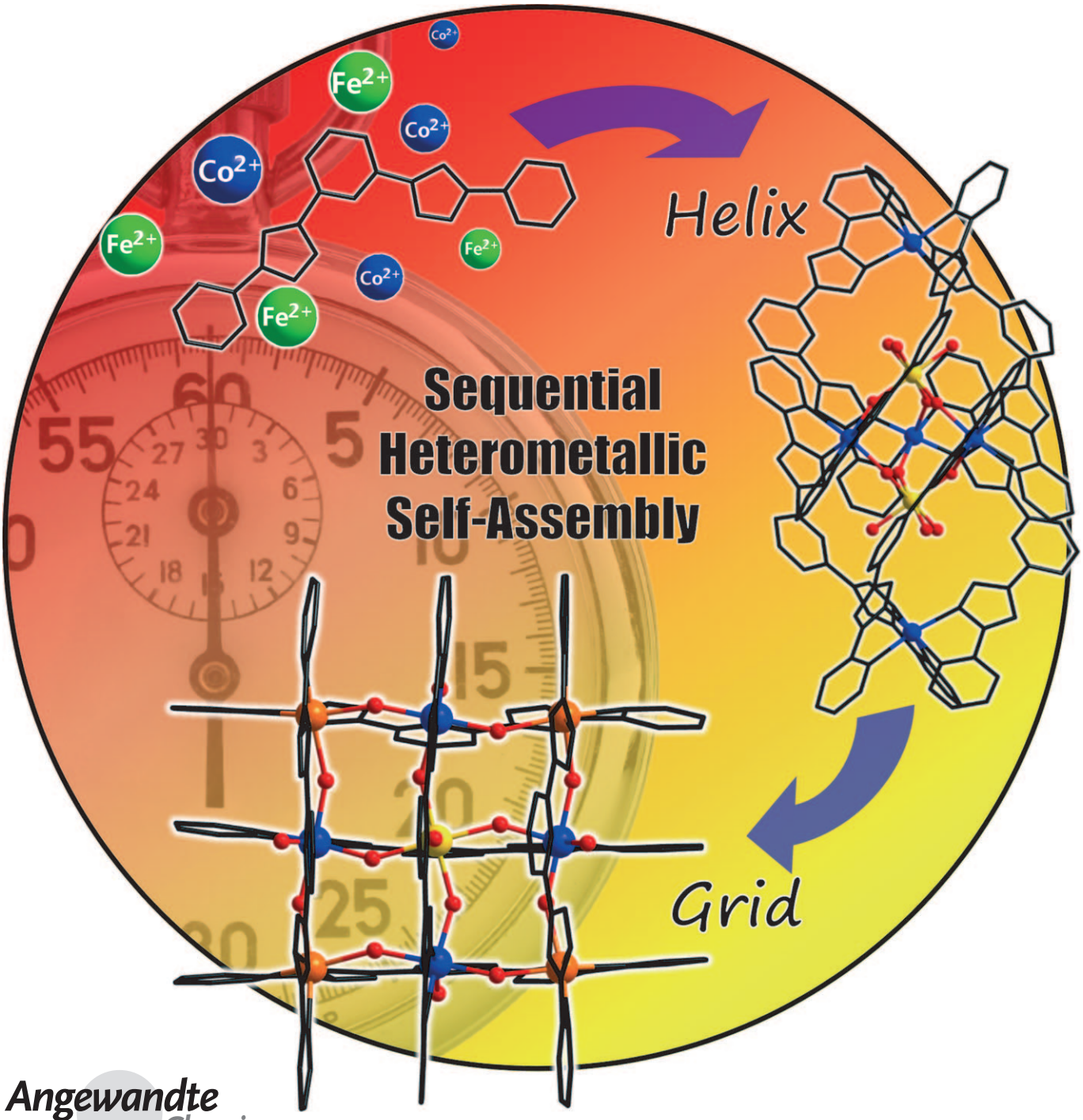

WILEY ONLINE LIBRARY

© 2011 Wiley-VCH Verlag GmbH & Co. KGaA, Weinheim

The study of polynuclear transition-metal clusters is an area of great interest owing to the potential of such compounds to exhibit architecture-dependent behavior, such as molecular magnetism and host–guest and catalytic properties.[1,2] One critical challenge is the multicomponent synthesis of nanoscale heterometallic cluster architectures, whereby different species with well-defined structures and physical properties can be isolated from one-pot solutions with a clear control parameter.[3]

One of the key approaches to gain a measure of control over the self-assembly process is to utilize a ligand system that provides both rigidity (to minimize variability) and multidenticity (to ensure multiple metal centers are coordinated).[4] Polypyridyl ligands are an important group of compounds that meet these criteria and have been successfully used in a range of coordination clusters, such as in the elegant cage syntheses of Fujita et al.,[5] the $[n \times n]$ grids of Lehn et al. and Thompson et al., amongst others,[6] and in the synthesis of molecular wires.[7] The specific arrangement of ions in these materials can induce multistabilities owing to spin-crossover[8] and mixed valency,[6c] and magnetic properties, such as single-molecule magnetism[6b] and quantum magnetic oscillation.[9] The synthesis of regular heterometallic arrays is an area of intense research, as the inclusion of different metals in a cluster can lead to drastic changes in the physical properties, such as the spin ground state and redox activity, through the alteration of the overall magnetic and electronic interactions.[10]

We have previously accomplished the synthesis of the first grid SMM; a $[3 \times 3]$ Co^{II}/Co^{III} array which showed slow magnetic relaxation.[6b] Herein, we use a similar architectural approach for the synthesis of mixed cobalt/iron clusters, resulting in the formation of heterometallic helix and grid complexes (Figure 1).

The polypyridine ligand H_2L (2,6-bis[5-(2-pyridinyl)-1*H*-pyrazole-3-yl]pyridine),[6b,11] consists of three pyridine groups linked by two pyrazole moieties, thus forming one tridentate and two bidentate binding sites. A heptanuclear helical complex, $[Fe^{III}_2Co^{II}_5(H_2L)_6O_6(H_2O)_6](BF_4)_4$ (**1**), was obtained by the reaction of $Fe(BF_4)_2{\cdot}6H_2O$ and $Co(BF_4)_2{\cdot}6H_2O$ in a 1:8 Fe/Co ratio, with H_2L and triethylamine in a 2:1 mixture of MeOH and MeCN under ambient conditions. The nonanuclear heterometallic grid complex $[Fe^{II}_4Fe^{III}Co^{II}_4(H_2L)_6{\cdot}(OH)_{12}(H_2O)_6](BF_4)_7$ (**2**) was obtained by the same procedure as **1** but using a 1:1 Fe/Co ratio. The formulae of both complex cations were confirmed by ESI-MS (Supporting Information, Figure S1).

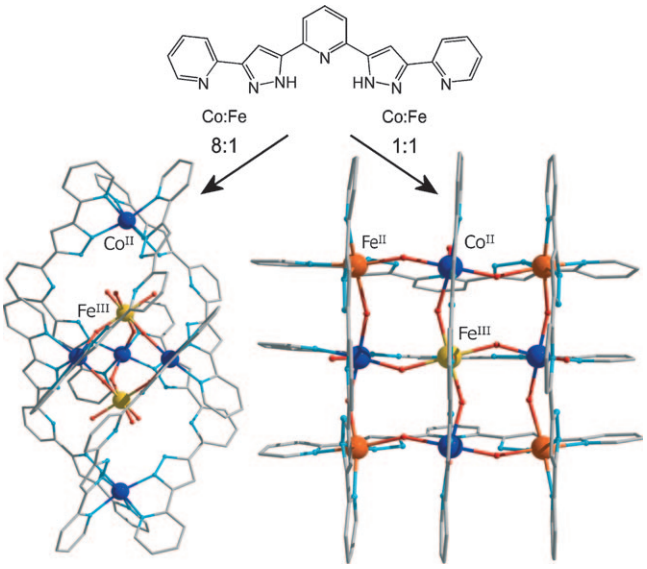

Figure 1. Crystal structures of clusters **1** (left) and **2** (right). C gray, N light blue, O red, Co^{II} dark blue, Fe^{III} yellow, Fe^{II} orange. Hydrogen atoms, counteranions, and solvent molecules are excluded for clarity.

Complex **1** has a helical structure and consists of six bis(bidentate) ligands, two Fe^{III} ions, and five Co^{II} ions, as confirmed by charge balance, structural arguments, and Mössbauer spectroscopy. Compound **1** has a pentanuclear core structure in which three Co^{II} centers form a planar triangular arrangement and are capped above and below the plane by two $[Fe^{III}O_3(OH_2)_3]^{3-}$ units from which each oxo ligand acts as a μ_2 bridge between the capping Fe^{III} ion and one Co^{II} center. The pentanuclear oxo core is capped by two distant divalent cobalt ions. The three central cobalt ions have $\{N_4O_2\}$ coordination environments in which they are coordinated by two bidentate ligand binding sites and two oxide ions, resulting in an octahedral coordination geometry with average Co–N and Co–O bonds of 2.135(4) and 2.024(3) Å, respectively. The two iron ions that complete the oxo-bridged core have octahedral coordination environments with three oxide ions and three water molecules with an average Fe–O bond of 1.932(3) Å. The final two cobalt ions, located at the extremities of the helical cluster, have octahedral $\{N_6\}$ donor sets through the coordination of three bidentate ligand binding sites with average Co–N bonds of 2.156(4) Å.

Complex **2** has a $[3 \times 3]$ grid structure and is composed of six ligands coordinating five iron and four cobalt ions, as confirmed by ICP measurements, in a bis(bidentate) manner. There are three kinds of metal center in the cluster, categorized as central, edge, and corner ions. All metal

[*] Dr. G. N. Newton, T. Onuki, Dr. T. Shiga, M. Noguchi, T. Matsumoto, Dr. M. Nihei, Prof. Dr. H. Oshio
Graduate School of Pure and Applied Sciences
University of Tsukuba
Tennodai 1-1-1, Tsukuba 305-8571 (Japan)
Fax: (+81) 29-853-4238
E-mail: oshio@chem.tsukuba.ac.jp
J. S. Mathieson, Prof. Dr. L. Cronin
Department of Chemistry, Joseph Black Building
University of Glasgow
University Avenue, Glasgow G12 8QQ (UK)
Fax: (+44) 141-330-4888
E-mail: lee.cronin@glasgow.ac.uk
Prof. Dr. M. Nakano
Department of Applied Chemistry, Graduate School of Engineering, Osaka University (Japan)

[**] This work was supported by a Grant in Aid for Scientific Research for Priority Area "Coordination Programming" (area 2107) from MEXT (Japan), the JSPS, the EPSRC, the University of Glasgow, and WestCHEM.

Supporting information for this article is available on the WWW under http://dx.doi.org/10.1002/anie.201007388.

 © 2011 Wiley-VCH Verlag GmbH & Co. KGaA, Weinheim

centers are bridged by μ_2-hydroxo ligands[12] where the central ion has four bridges to neighboring cations, the edge ions three, and the corner ions two. Compositional arguments suggest that one trivalent and eight divalent metal ions form the complex cation. Mössbauer, magnetic susceptibility, and structural data allowed us to deduce that high-spin (HS) Fe^{III}, intermediate-spin (IM) Fe^{II}, and HS Co^{II} ions were present and located at the center, corners, and edges, respectively (see below). The central Fe^{III} ion has octahedral coordination geometry consisting of four μ_2-OH ligands and two water molecules with bonding interactions that average 1.966(4) Å. The four edge metal centers have $\{N_2O_4\}$ octahedral coordination environments in which they are in the weak ligand field of one bidentate ligand site, three μ_2-OH groups, and one water molecule, with average M–N and M–O bonds of 2.155(6) and 1.914(5) Å, respectively, which are reasonable values for Co^{II} ions. The four corner ions have multiaxially distorted $\{N_4O_2\}$ octahedral environments in which two bidentate ligand sites and two hydroxide ions coordinate, with average M–N and M–O bonds of 2.099(7) and 2.075(4) Å, respectively, which are too long for LS metal centers but acceptable for HS or IM ions (Supporting Information, Figure S2). It is reasonable to assign the edge and corner metal ions as HS Co^{II} ($S=3/2$) and IM Fe^{II} ($S=1$) ions, respectively.[13,14]

The configurations of both clusters result from intramolecular hydrogen-bonding interactions. The central tridentate ligand site does not coordinate to a metal center, but instead forms hydrogen-bonding interactions with metal-coordinating water ligands. This suggests that despite its planar, rigid nature, the ligand is not a classical "directing" ligand, and in fact relies upon weak interactions to stabilize the architectures of both clusters.

The Mössbauer spectrum of **1** at 10 K consists of a single quadrupole doublet with $\delta=0.55$ and $\Delta E_Q=0.20\ mm\,s^{-1}$ (relative to metallic iron), which is characteristic of HS Fe^{III}. In contrast, measurements of **2** (conducted at 20, 100, 200, and 300 K) showed two quadrupole doublets with a peak area ratio of 1:4. The Mössbauer parameters of the small doublet at 20 K were $\delta=0.47$ and $\Delta E_Q=0.17\ mm\,s^{-1}$, which is characteristic of HS Fe^{III}, thus confirming the assignment of the central HS Fe^{III} ion. The larger doublet ($\delta=0.49$ and $\Delta E_Q=0.33\ mm\,s^{-1}$) can be interpreted as representing four LS or IM Fe^{II} centers;[14a] however, magnetic susceptibility measurements and consideration of the bond lengths suggest that the four iron ions in **2** are in the IM state and located on the corners of the grid. Note that no HS Fe^{II} doublet was observed at any temperature (Supporting Information, Figure S3 and S4).

Magnetic susceptibility data for **1** and **2** were collected over the temperature range of 1.8–300 K under an applied field of 500 Oe (Supporting Information, Figure S5). The $\chi_m T$ value for **1** was 18.62 emu mol^{-1} K at 300 K, which is slightly larger than the value (18.13 emu mol^{-1} K) expected for the sum of the Curie constants of two $Fe^{III}{}_{HS}$ ions ($S=5/2$) and five $Co^{II}{}_{HS}$ ions ($S=3/2$). As the temperature was lowered, the $\chi_m T$ values gradually decreased, reaching a minimum value of 3.74 emu mol^{-1} K at 1.8 K. The $\chi_m T$ value for **2** was 18.17 emu mol^{-1} K at 300 K, which is larger than that (15.88 emu mol^{-1} K) expected for one $Fe^{III}{}_{HS}$ ion ($S=5/2$), four $Fe^{II}{}_{IM}$ ions ($S=1$), and four $Co^{II}{}_{HS}$ ions ($S=3/2$) owing to the contribution of spin–orbit coupling that leads to large g values. The existence of four $Fe^{II}{}_{HS}$ in place of the $Fe^{II}{}_{IM}$ can be discounted as they would lead to a $\chi_m T$ value of 23.88 emu mol^{-1} K, however, $Fe^{II}{}_{LS}$ ions remain a possibility as the calculated $\chi_m T$ value of 11.88 emu mol^{-1} K could correspond to the data if $g_{Co}{}^{II}=2.47$. The $\chi_m T$ values gradually decreased with temperature, reaching a minimum of 0.40 emu mol^{-1} K at 1.8 K. The magnetic susceptibility data of **1** and **2** were fitted using HDVV spin Hamiltonians, yielding average g values of 2.08 and 2.20 respectively, with $J_{Co-Fe^{III}}=-10.6$ K in **1**, and $J_{Co-Fe^{II}}=-19.8$ K and $J_{Co-Fe^{III}}=-16.8$ K in **2** (Supporting Information, Figure S6). The data confirm that antiferromagnetic interactions are dominant in both **1** and **2**. This is critical in the analysis of **2**, as this antiferromagnetic behavior strongly suggests that the edge positions hold paramagnetic ions, in agreement with their assignment as Co^{II}.[6e] The combination of analytical techniques allows us to assign the corner ions in **2** as $Fe^{II}{}_{IM}$; with bond lengths ruling out $Fe^{II}{}_{LS}$ ions, and the magnetic and Mössbauer data discounting the possibility that they are $Fe^{II}{}_{HS}$ ions.

To probe the behavior of the compounds in the solution/gas phase, ESI-MS measurements were conducted on MeOH/MeCN (2:1) solutions of crystals of **1** and **2** at 180 °C. Both clusters could be identified with envelopes corresponding to $[Fe^{III}{}_2Co^{II}{}_5(H_2L)_6O_6(H_2O)_2(BF_4)_2(MeOH)_3]^{2+}$ observed at m/z 1500.3 (fit: 1500.2) for **1**, and $[Fe^{II}{}_5Co^{II}{}_4(H_2L)_6(OH)_{14}(MeOH)_3(BF_4)_2]^{2+}$ at m/z 1607.8 (1607.7) for **2** (Supporting Information, Figure S1). Despite the presence of different structural motifs, the synthetic approach to **1** and **2** is almost identical, relying only on the starting ratio of the metal salts to determine which product is favored. To investigate the self-assembly processes in action which lead to the different crystalline products, preliminary ESI-MS studies were conducted on the reaction mixture after mixing, as a function of time. To accomplish this, samples of the reaction solutions were taken every two minutes, and the spectra monitored to investigate the self-assembly processes underway. The reaction solution of complex **1** showed the initial formation of the helix minus one ligand (0 min) but displayed little change over time, with the exception of the appearance of some lower nuclearity peaks (Supporting Information, Figure S7). This formation of the expected complex minus one ligand may be due to the species having greater (dilute) solution stability than the intact cluster.

In contrast, the time-resolved ESI-MS investigation of the assembly of **2** shows the gradual growth of possible structural building blocks, as observed in the gas phase (Figure 2; Supporting Information, Figure S8). The spectrum at $t=$ 0 min showed that, amongst the most prominent peaks, were those representing generally simple clusters, such as $[Fe^{II}{}_2Co^{II}{}_3(H_2L)_5O_2(OH)_3(H_2O)(CH_3OH)_2]^{3+}$ at m/z 760.1 (760.1), $[Co^{III}Co^{II}(H_2L)_3(OH)_2O]^{+}$ at m/z 1263.3 (1263.3), and $[Fe^{III}Fe^{II}Co^{II}\ (H_2L)_3O_2(CH_3O)_2]^{+}$ at m/z 1360.2 (1360.2). Surprisingly, the formation of the intact cluster **1** was also observed in the initial measurements at $[Fe^{III}{}_2Co^{II}{}_5(H_2L)_6O_6(CH_3O)]^{3+}$ at m/z 908.5 (908.5) and $[Fe^{III}{}_2Co^{II}{}_5(H_2L)_6O_6(BF_4)_2(H_2O)_2(CH_3OH)_3]^{2+}$ at m/z 1500.3 (1500.3) (note that

 © 2011 Wiley-VCH Verlag GmbH & Co. KGaA, Weinheim

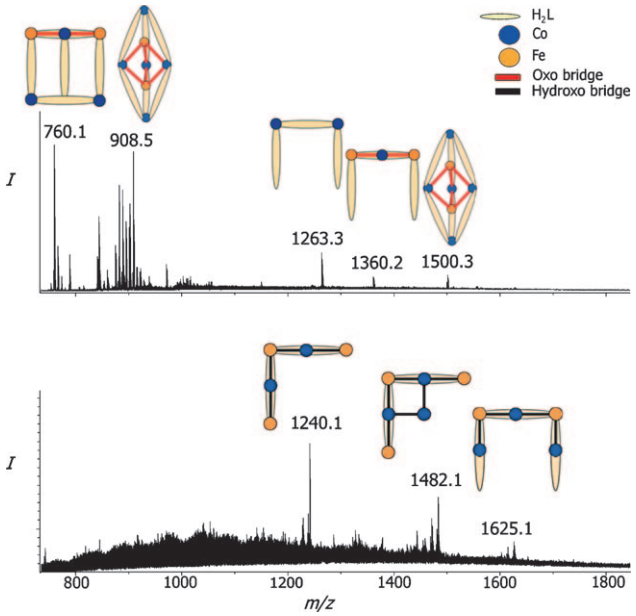

Figure 2. ESI-MS spectra of **2** at $t = 0$ min (top) and 14 min (bottom) and speculative structures based on peak fitting.

there was no cross-contamination between samples), suggesting some commonality between the assemblies of **1** and **2**. After 14 minutes, the spectrum had changed significantly and contained new cluster peaks, which appeared to correspond to portions of the final product **2**, such as $[Fe^{II}_2Fe^{III}Co^{II}_2(H_2L)_2(OH)_{10}(H_2O)_3]^+$ at *m/z* 1240.1 (1240.0), $[Fe^{III}_2Fe^{II}Co^{II}_3(H_2L)_2O_3(OH)_7(H_2O)_8(CH_3OH)_3]^+$ at *m/z* 1482.1 (1482.0), and $[Fe^{III}_2Co^{II}_3(H_2L)_3(OH)_{11}(H_2O)_3]^+$ at *m/z* 1625.1 (1625.1). After 7 days, numerous peaks corresponding to a range of oxidation and solvation species of cluster **2** were present (Supporting Information, Figure S9).

Initial data from the time-dependent measurements suggested that the helical complex **1** may be an intermediate of **2**, so a further experiment was conducted to investigate this possibility. Crystals of **1** were dissolved in a 2:1 mixture of MeOH and MeCN and ESI-MS spectra collected. Subsequently, an excess of $Fe(BF_4)_2{\cdot}6H_2O$ was added to the same solution and the data re-collected. The resultant spectrum showed many additional peaks to those visible in the original measurement, and critically, appeared to show peaks which corresponded to the grid complex **2** (Supporting Information, Figure S10). Thus, we can suggest that **1** is an initially favored species, or reaction intermediate, in the synthesis of **2**, the isolation or decomposition of which is determined by the ratio of metal ions in solution. It is interesting to note that the role of **1** as an intermediate in the synthesis of **2** suggests that the oxidation state of the iron ions is variable in solution and depends upon the coordination environment in which they exist, with the O_6 donor sets stabilizing Fe^{III} and the N_4O_2 sets supporting Fe^{II} ions.

In conclusion, two new heterometallic clusters have been synthesized through subtle alterations to a simple one-pot approach. The structures show radically different motifs, despite the use of identical substituents. Time-resolved ESI-MS experiments to follow the self-assembly processes suggest that the helix **1** is formed initially in the synthesis of the grid **2**, before firstly being replaced by building blocks that can be tentatively assigned to be present in **2**, and eventually by the intact cluster core of **2**. Additional experiments showed that **2** could be observed by ESI-MS after addition of Fe^{II} ions to dissolved crystals of **1**, confirming the role of **1** as a stable intermediary in the synthesis of **2**. In future studies, we will explore how to generalize this approach in an effort to design routes to the assembly of coordination clusters with desired architectures and physical properties.

Experimental Section

Synthesis of **1**: A solution of $Fe(BF_4)_2{\cdot}6H_2O$ (33.8 mg, 0.1 mmol) and $Co(BF_4)_2{\cdot}6H_2O$ (272.5 mg, 0.8 mmol) in methanol (15 mL) were added to a mixture of H_2L (87.6 mg, 0.24 mmol) and triethylamine (66 μL, 0.48 mmol) in methanol (10 mL). The mixture was stirred for several minutes after addition of acetonitrile (13 mL). After a few days at room temperature, orange-red plate crystals of $[Fe_2Co_5(H_2L)_6O_6(H_2O)_6](BF_4)_4{\cdot}5H_2O{\cdot}7MeCN{\cdot}6MeOH$ (**1**·$5H_2O$·7MeCN·6MeOH) formed. Yield: 4.75%; Anal. calcd (%) for $C_{126}H_{112}B_4Co_5F_{16}Fe_2N_{42}O_{17}$ (**1**·$5H_2O$): C 46.71, H 3.48, N 18.16; found: C 46.38, H 3.14, N 18.20. ICP calcd: Fe 2.00, Co 5.00; found: Fe 2.03, Co 4.97.

Synthesis of **2**: A solution of $Fe(BF_4)_2{\cdot}6H_2O$ (151.9 mg, 0.45 mmol) and $Co(BF_4)_2{\cdot}6H_2O$ (153.3 mg, 0.45 mmol) in MeOH/MeCN (2:1 (v/v), 20 mL) was added to a mixture of H_2L (109.6 mg, 0.3 mmol) and triethylamine (83.5 μL, 0.6 mmol) in MeOH/MeCN (2:1 (v/v), 20 mL). The mixture was stirred for several minutes. After a few days, the resulting dark red-brown solution gave yellow plate crystals of $[Fe_5Co_4(H_2L)_6(OH)_{12}(H_2O)_6](BF_4)_7{\cdot}3H_2O{\cdot}4MeCN{\cdot}2MeOH$ (**2**·$3H_2O$·4MeCN·2MeOH). Yield: 23.5%; Anal. calcd (%) (found) for $C_{126}H_{120}N_{42}B_7Co_4F_{28}Fe_5O_{21}$ (**2**·$3H_2O$): C 41.08, H 3.26, N 15.97; found: C 41.92, H 3.10, N 16.05. ICP calcd: Fe 5.00, Co 4.00; found: Fe 5.08, Co 3.92.

Crystal data for **1**: red plate crystals, $C_{146}H_{157}B_4Co_5F_{16}Fe_2N_{49}O_{23}$, $M_r = 3718.81$, monoclinic, $C2/c$, $a = 30.061(4)$, $b = 32.943(4)$, $c = 32.945(4)$ Å, $\beta = 104.019(2)$, $V = 32222(7)$ Å^3, $Z = 8$, $d_{cal} = 1.618$ mg m^{-3}, μ(Mo Kα) $= 0.797$ mm^{-1}, $T = 100$ K, $R1 = 0.076$, $wR2 = 0.22$ ($I > 2\sigma$). Crystal data for **2**: yellow, $C_{136}H_{140}B_7Co_4F_{28}Fe_5N_{46}O_{23}$, $M_r = 3909.45$, triclinic, $P\bar{1}$, $a = 18.696(7)$, $b = 18.777(7)$, $c = 23.307(9)$ Å, $\alpha = 95.816(7)$, $\beta = 100.332(7)$, $\gamma = 105.695(7)°$, $V = 7651(5)$ Å^3, $Z = 2$, $d_{cal} = 1.676$ mg m^{-3}, μ(Mo Kα) $= 1.003$ mm^{-1}, $T = 100$ K, $R1 = 0.083$, and $wR2 = 0.240$ ($I > 2\sigma$). Both data sets were treated with the SQUEEZE program to remove highly disordered solvent molecules, and one counteranion in the case of **2**. The crystallographic formulae include the number of solvent molecules suggested by SQUEEZE (see cif files). CCDC 791525 and 791526 contain the supplementary crystallographic data for this paper. These data can be obtained free of charge from The Cambridge Crystallographic Data Centre via www.ccdc.cam.ac.uk/data_request/cif.

Received: November 24, 2010
Revised: January 19, 2011
Published online: February 25, 2011

Keywords: cobalt · iron · mass spectrometry · self-assembly · spin states

[1] a) D. Gatteschi, R. Sessoli, J. Villain, *Molecular Nanomagnets*, Oxford Press, New York, **2006**; b) M. Yoshizawa, M. Tamura, M. Fujita, *Science* **2006**, *312*, 251.

 © 2011 Wiley-VCH Verlag GmbH & Co. KGaA, Weinheim

[2] a) S. Leininger, B. Olenyuk, P. J. Stang, *Chem. Rev.* **2000**, *100*, 853; b) M. Fujita, *Chem. Soc. Rev.* **1998**, *27*, 417.
[3] a) J.-M. Lehn, *Supramolecular Chemistry: Concepts and Perspectives*, VCH, Weinheim, **1995**; b) P. Mal, D. Schultz, K. Beyeh, K. Rissanen, J. R. Nitschke, *Angew. Chem.* **2008**, *120*, 8421; *Angew. Chem. Int. Ed.* **2008**, *47*, 8297.
[4] a) G. L. Wang, X. L. Yang, Y. Liu, Y. Z. Li, H. B. Du, X. Z. You, *Inorg. Chem. Commun.* **2008**, *11*, 814; b) I. M. Müller, T. Röttgers, W. S. Sheldrick, *Chem. Commun.* **1998**, 823.
[5] M. Yoshizawa, J. K. Klosterman, M. Fujita, *Angew. Chem.* **2009**, *121*, 3470; *Angew. Chem. Int. Ed.* **2009**, *48*, 3418.
[6] a) L. K. Thompson, O. Waldmann, Z. Xu, *Coord. Chem. Rev.* **2005**, *249*, 2677; b) T. Shiga, T. Matsumoto, M. Noguchi, T. Onuki, N. Hoshino, G. N. Newton, M. Nakano, H. Oshio, *Chem. Asian J.* **2009**, *4*, 1660; c) E. Breuning, M. Ruben, J.-M. Lehn, F. Renz, Y. Garcia, V. Ksenofontov, P. Gütlich, E. Wegelius, K. Rissanen, *Angew. Chem.* **2000**, *112*, 2563; *Angew. Chem. Int. Ed.* **2000**, *39*, 2504; d) M. Ruben, J. Rojo, F. J. Romero-Salguero, L. H. Uppadine, J.-M. Lehn, *Angew. Chem.* **2004**, *116*, 3728; *Angew. Chem. Int. Ed.* **2004**, *43*, 3644, and references therein; e) L. N. Dawe, K. V. Shuvaev, L. K. Thompson, *Inorg. Chem.* **2009**, *48*, 3323, and references therein.
[7] C. Yin, G.-C. Huang, C.-K. Kuo, M.-D. Fu, H.-C Lu, J.-H. Ke, K.-N. Shih, Y.-L. Huang, G.-H. Lee, C.-Y. Yeh, C.-h. Chen, S.-M. Peng, *J. Am. Chem. Soc.* **2008**, *130*, 10090.
[8] B. Schneider, S. Demeshko, S. Dechert, F. Meyer, *Angew. Chem.* **2010**, *122*, 9461; *Angew. Chem. Int. Ed.* **2010**, *49*, 9274.
[9] O. Waldmann, S. Carretta, P. Santini, R. Koch, A. G. M. Jansen, G. Amoretti, R. Caciuffo, L. Zhao, L. K. Thompson, *Phys. Rev. Lett.* **2004**, *92*, 096403.
[10] T. Matsumoto, T. Shiga, M. Noguchi, T. Onuki, G. N. Newton, N. Hoshino, M. Nakano, H. Oshio, *Inorg. Chem.* **2010**, *49*, 368.
[11] I. G. Phillips, P. J. Steel, *Inorg. Chim. Acta* **1996**, *244*, 3.
[12] BVS calculations for OH ligands in **2**: O1 1.06, O2 1.06, O3 1.05, O4 1.07, O5 0.98, O6 0.88, O7 0.87, O8 0.96, O9 0.99, O10 0.90, O11 0.89, O12 0.99.
[13] A. Nabei, T. Kuroda-Sowa, T. Okubo, M. Maekawa, M. Munakata, *Inorg. Chim. Acta* **2008**, *361*, 3489.
[14] a) D. C. Figg, R. H. Herber, I. Felner, *Inorg. Chem.* **1991**, *30*, 2535; b) E. Koenig, K. Madeja, *Inorg. Chem.* **1968**, *7*, 1848; c) E. Konig, K. Madeja, *J. Am. Chem. Soc.* **1966**, *88*, 4528.

 © 2011 Wiley-VCH Verlag GmbH & Co. KGaA, Weinheim